NANO LETTERS

Letter

pubs.acs.org/NanoLett

Interplay Between Structure, Stoichiometry, and Electron Transfer Dynamics in SILAR-based Quantum Dot-Sensitized Oxides

Hai Wang,[†,‡] Irene Barceló,[§] Teresa Lana-Villarreal,[§] Roberto Gómez,[§] Mischa Bonn,[†] and Enrique Cánovas*[,†,∥]

[†]Max Planck Institute for Polymer Research, Ackermannweg 10, 55128 Mainz, Germany

[‡]Graduate School of Material Science in Mainz, University of Mainz, Staudingerweg 9, 55128 Mainz, Germany

[§]Institut Universitari d'Electroquímica i Departament de Química Física, Universitat d'Alacant, Apartat 99, E-03080 Alacant, Spain

[∥]FOM Institute for Atomic and Molecular Physics, Science Park 104, 1098 XG Amsterdam, The Netherlands

S *Supporting Information*

ABSTRACT: We quantify the rate and efficiency of picosecond electron transfer (ET) from PbS nanocrystals, grown by successive ionic layer adsorption and reaction (SILAR), into a mesoporous SnO_2 support. Successive SILAR deposition steps allow for stoichiometry- and size-variation of the QDs, characterized using transmission electron microscopy. Whereas for sulfur-rich (p-type) QD surfaces substantial electron trapping at the QD surface occurs, for lead-rich (n-type) QD surfaces, the QD trapping channel is suppressed and the ET efficiency is boosted. The ET efficiency increase achieved by lead-rich QD surfaces is found to be QD-size dependent, increasing linearly with QD surface area. On the other hand, ET rates are found to be independent of both QD size and surface stoichiometry, suggesting that the donor−acceptor energetics (constituting the driving force for ET) are fixed due to Fermi level pinning at the QD/oxide interface. Implications of our results for QD-sensitized solar cell design are discussed.

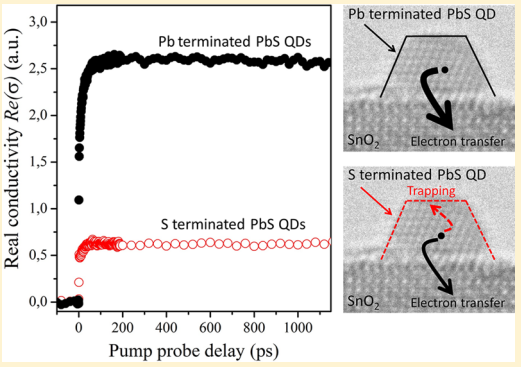

KEYWORDS: *Quantum dot stoichiometry, SILAR, PbS quantum dots, epitaxial growth, electron transfer, THz spectroscopy, quantum dot-sensitized solar cells*

The sensitization of wide bandgap oxides by quantum dots (QDs) represents a promising route for the development of low-cost solar energy conversion devices (e.g., photovoltaics[1−6] and photocatalysis[7−9]). The QD synthesis can be performed either ex situ, that is, colloidal dots are prepared and then directly adsorbed on or molecularly linked to the oxide,[2] or in situ, with nanocrystals directly nucleated and grown onto the oxide matrix,[3,4,10] for example, through chemical bath deposition (CBD)[11,12] or successive ionic layer adsorption and reaction (SILAR).[13] The ex situ approach provides a path for obtaining highly monodisperse QDs but commonly suffers from the formation of QD aggregates and/or limited QD surface coverage (constrained by oxide pore size). Electronically, the QD capping shell and/or the molecular bridges linking the QDs to the oxide can act as an insulating barrier to electron transfer; for aromatic and aliphatic molecular bridges, charge transfer has been shown to proceed via coherent tunneling, slowing down with increasing bridge length.[14] On the other hand, in situ QD sensitization potentially enables heteroepitaxial growth that allows morphologically well-defined QD donors[15−18] and can offer larger QD surface coverages in mesoporous oxide architectures compared to the ex situ approaches. Moreover, the intimate QD/oxide contact is expected to provide the strongest achievable electronic coupling for a given donor/acceptor system. This particular property could enable ultrafast and efficient QD-to-oxide ET processes at little to no energy cost, reaching the ultimate theoretical ∼30% Shockley-Queisser limit for photon-to-electron energy conversion in sensitized systems.[19]

Previous reports on in situ nucleated QDs, however, have suggested wide QD size distributions and a lack of control over the nanocrystal morphology.[17] This has been primarily concluded from the featureless QD optical response, which can also be an intrinsic manifestation of the strong donor−acceptor electronic wave function overlap.[20,21] Among the existing in situ methodologies, the SILAR method allows low-temperature-solution-processed epitaxial thin film growth[22,23] and SILAR-based QD-sensitized solar cells with efficiencies exceeding 5% have been reported.[3,6] The strengths of the SILAR approach to grow QDs on metal oxides lie in the fact that (i) the size of the QD can be controlled to some extent by the number of deposition cycles[24,25] and (ii) the QD surface stoichiometry can be easily tuned,[26] opening new possibilities for QD doping[27−30] and providing a path for atomically

Received: July 14, 2014
Revised: September 16, 2014
Published: September 19, 2014

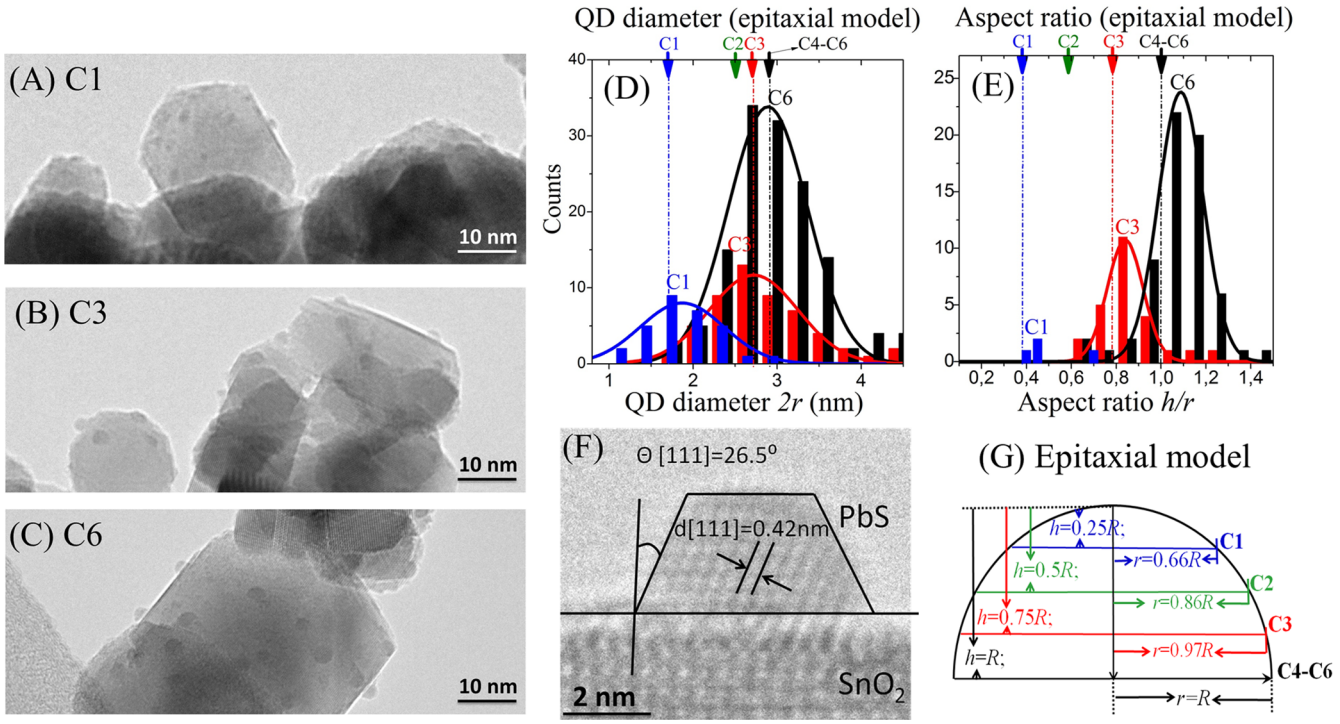

Figure 1. (A–C) Characteristic TEM images for SnO_2 samples sensitized with 1, 3, and 6 SILAR cycles (C1, C3, and C6, respectively); (D) histograms of QD base diameters ($2r$) as a function of SILAR cycles (vertical bars) and results of the semiempirical nucleation model (dashed vertical lines) shown in panel (G); (E) histograms of QD aspect ratios (vertical bars) and comparison with the semiempirical nucleation model (dashed vertical lines) shown in panel (G). (F) [111] faceted epitaxial PbS QD resolved by TEM at the SnO_2 edge; (G) proposed nucleation mechanism ("epitaxial model") for spherical cap-shaped QDs sensitizing a mesoporous oxide by SILAR method (h and r denotes QD height and base radius, R refers to the saturated QD radius when h/r aspect ratio is unity).

passivated dots.[31] Additionally, highly monodisperse core/shell colloidal QDs can be obtained when this sensitization methodology is applied.[32] Despite the apparent potential of this approach, several important questions concerning SILAR-based QD-sensitized oxides remain open; clear correlations between chemical synthesis, QD structure and stoichiometry, donor–acceptor charge transfer dynamics and their impact on device performance are lacking.

Here, we investigate the interplay between QD structure, stoichiometry, and electron transfer rate and efficiency in SILAR-based PbS QD-sensitized tin oxides as a function of SILAR deposition steps. Transmission electron microscopy (TEM) analysis indicates that the size of PbS QDs is controlled through sequential epitaxial deposition steps, as is the stoichiometry. Optical pump-THz probe (OPTP) spectroscopy reveals electron transfer (ET) rates independent of QD size and surface chemistry, indicative of Fermi level pinning at the QD/oxide interface. In contrast to the ET rate, the ET efficiency from PbS and PbSe QDs directly nucleated onto a mesoporous oxide (SnO_2, TiO_2, and ZnO) is very sensitive to the QD surface composition, being substantially enhanced for lead-rich surfaces. Finally, we correlate our OPTP photoconductivity measurements with photocurrent generation in QD-sensitized solar cells (QDSSCs), highlighting the relevance of our observations for solar cell design.

We characterize ET processes on QD-sensitized oxides using OPTP spectroscopy[14,33−37] with subpicosecond time resolution. Owing to its low photon energy, terahertz (THz) radiation is insensitive to optical transitions in QDs;[34,37] however, because the THz probe is absorbed by mobile carriers populating the oxide conduction band, the photoinduced THz absorption is directly related to the photoconductivity of the sample. Hence, following optical excitation of the QD, the time-dependent pump-induced absorption of the THz probe in a QD-sensitized system can be directly correlated with ET from the QDs to the oxide.[14,33,35,36] Note that not only the ET rate but also the efficiency of the ET process can be obtained from OPTP measurements, through the amplitude of the photo-induced THz absorption (more details are given in the Supporting Information Figures S4 and S5).

Sensitization of a mesoporous SnO_2 matrix with PbS QDs was achieved by alternatively dipping the oxide film (up to 6 times) into beakers containing a (i) MeOH-based $Pb(NO_3)_2$ solution, providing the Pb^{2+} cations, (ii) pure MeOH solvent to remove the excess of unbound cations, (iii) MeOH-based Na_2S solution, providing the S^{2-} anions, and (iv) pure MeOH solvent to remove the excess of unbound anions. Steps (i)–(iv) are termed as one SILAR cycle and are denoted here as Cn, $n \geq 1$. Analogously, we define here half-cycle as the same routine terminated after step (ii) (a scheme of SILAR method is given in the Supporting Information, Figure S1). Note that half-cycle samples (Cn.5, $n \geq 1$) are characterized by a Pb-rich surface while samples grown with a complete cycle (Cn, $n \geq 1$) are S-rich. To avoid QD photo-oxidation (see Figure S7 in Supporting Information), sample preparation and measurements were realized under N_2 conditions. More details about the sample preparation as well as the OPTP measurement protocol are provided in the Supporting Information.

Before reporting how QD stoichiometry affects electron transfer rate and efficiency, we characterize the SILAR-grown nanocrystal morphologies.

dx.doi.org/10.1021/nl5026634 | Nano Lett. 2014, 14, 5780−5786

QD Growth Mechanism. The characteristic red shift of the absorption threshold of SILAR-based QD-sensitized oxides versus the number of SILAR cycles[24,25] is a manifestation of a size-dependent confinement effect (see Figure S2 in Supporting Information for our samples). In order to accurately correlate QD structure and ET dynamics, we performed transmission electron microscopy on our samples; representative images for PbS QDs on a SnO_2 mesoporous support for samples C1, C3, and C6 are shown in Figure 1A–C. The TEM images reveal that QDs are uniformly distributed on the oxide surfaces and do not show preferential nucleation on particular SnO_2 facets (larger area and higher resolution images are provided in the Supporting Information, Figure S3). From TEM image statistical analysis, a saturation of PbS QD base diameter ($2r$) is apparent for samples beyond 3 SILAR cycles (see Figure 1D). The saturation in QD base diameter is followed by a significant change in QD height (as resolved by monitoring QD aspect ratios (h/r), as a function of the number of SILAR cycles, see Figure 1E). A similar qualitative change in aspect ratios was reported before for SILAR-based CdSe QDs onto TiO_2 and ZnO surfaces.[13,38] In parallel with the saturation of the QD base diameter (from C3 and onward), we observe the emergence of QD aggregates (PbS bulky phases, see TEM images in Supporting Information Figure S3D,F). The emergence of polycrystalline PbS phases after the QDs saturate in base diameter is consistent with the appearance of an ultrafast component in the ET dynamics for samples beyond C4 due to direct photogeneration and recombination of free carriers within the bulky QD clusters (see Figure S8A,B in Supporting Information). Similar behavior has previously been observed for samples sensitized with colloidal QDs.[14,33,35] Furthermore, the emergence of an ultrafast component on the OPTP dynamics is accompanied in our samples by a decrease in the ET efficiency (as apparent from the reduced THz response at long times, see Figure S8A, Supporting Information), indicating that the PbS bulky patches are strong photon absorbers but are not substantially contributing to the overall photocurrent in the samples. This scenario agrees well with previous observations that QDSSCs typically exhibit an increase in photocurrent followed by a decrease, as a function of the number of SILAR cycles.[24,25] The correlation between nanostructure and ET dynamics stresses the importance of preventing the transition from isolated QD growth to polycrystalline thin film growth in sensitized architectures. For an optimum device performance, high surface densities of isolated QDs without aggregate formation are required.

Heteroepitaxial QD/oxide growth by different solution-processing methods has recently been discussed in a review;[17] concerning the SILAR method, to the best of our knowledge only one report resolved the epitaxial growth of crystalline PbS QDs nucleated onto anatase TiO_2 surfaces by TEM.[25] As shown in Figure 1F, for our samples we have also been able to resolve crystalline PbS QDs epitaxially grown onto rutile SnO_2 surfaces. Our deposition recipe results in [111] faceted PbS dots with near-unity aspect ratio. These observations, together with the characteristic change in QD aspect ratio as a function of deposited material, indicate that epitaxial growth (triggered by QD/oxide lattice mismatch) most likely governs the nucleation of nanocrystals in our SILAR-based samples. Note that in heteroepitaxial Volmer–Weber growth mode an increasing aspect ratio as a function of the amount of deposited material has been predicted theoretically[39] and resolved experimentally.[40,41] Based on this analogy, we propose a simple model for the growth kinetics as sketched in Figure 1G. Our semiempirical model considers spherical cap-shaped QDs assuming that SILAR deposition steps change the height of the QDs linearly and that the QD growth is self-limiting when h/r aspect ratios approach unity (half-sphere shaped QDs). Taking only the empirically measured saturated QD diameter radius as input ($R = r \sim 2.9$ nm for C6), such a simple growth model is able to describe remarkably well the QD diameters ($2r$) and aspect ratios (r/h) obtained from our statistical treatment on TEM characterization (see dashed lines in Figure 1D,E).

Dependence of ET Rates on QD Size and Stoichiometry. Once the QD size dependence on the number of SILAR cycles has been resolved and modeled, we analyze the ET rates. Figure 2A shows the normalized pump-induced real part of the complex THz photoconductivity ($\mathrm{Re}(\sigma)$) for samples C1, C2, and C3. The rise of the signal after photoexcitation is a direct manifestation of ET from the QD donor to the oxide acceptor, as the conductivity of electrons (and holes) in the QD is purely imaginary.[41] As shown in the plot, the observed ET dynamics in all cases are identical within the signal-to-noise ratio of our measurements, indicating that electron transfer rates from the sensitizer to the oxide are independent of the QD size. On the other hand, as shown in the inset of Figure 2A, the back-transfer, resulting in recombination of electrons and holes, does slow down with the number of SILAR cycles. A simple model using a single-stretched-exponential ingrowth and decay reveals rates of ET from QD to oxide and back electron transfer (BET) from oxide to QD (K_{ET} and K_{BET}, respectively) of $1/K_{ET}$(C1–3) = 6.5 ± 1.5 ps (with stretched coefficients of 0.68 ± 0.05) and $1/K_{BET}$ (C1) = 2650 ± 140 ps, $1/K_{BET}$(C2) = 4620 ± 160 ps, and $1/K_{BET}$ (C3–C3.5) = 8100 ± 500 ps. Interestingly, as shown in Figure 2B, the ET dynamics are independent (within the resolution of our measurements, see Supporting Information) not only of cycle number but also of QD stoichiometry as illustrated by the OPTP traces for samples C3 and C3.5 (characterized by sulfur- and lead-rich QD surfaces, respec-

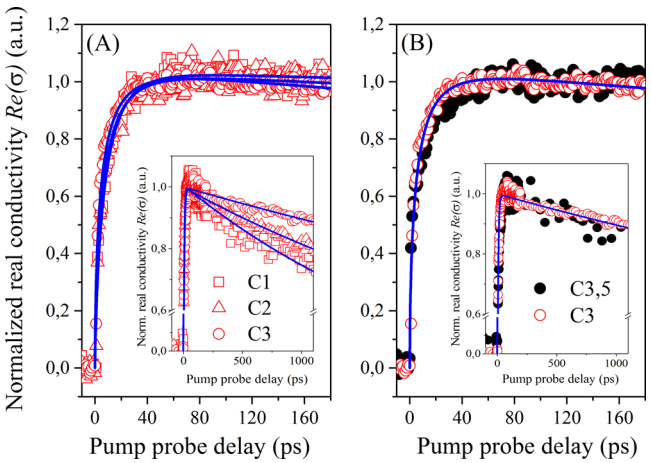

Figure 2. (A) Normalized OPTP response for PbS QDs sensitizing SnO_2 as a function of the number of SILAR cycles (Cn, with n = 1–3); in the inset are shown the dynamics up to 1.1 ns; blue lines are best fits to the data as described in the text. (B) Normalized OPTP response for PbS QDs sensitizing SnO_2 by SILAR as a function of surface stoichiometry (by comparing samples with C3 and C3.5 SILAR cycles, sulfur- and lead-rich, respectively); the inset shows the dynamics up to 1.1 ns; blue lines are best fits to the data.

dx.doi.org/10.1021/nl5026634 | Nano Lett. 2014, 14, 5780–5786

tively). The fact that back ET rates are independent of QD stoichiometry suggests that the QD-oxide energetics and coupling strength are independent of QD surface doping. The invariance of ET dynamics with QD size and stoichiometry can be rationalized by Fermi level pinning[42,43] at the PbS/SnO_2 interface, so that the energy difference between QD LUMO and oxide CB (given by ΔG and $\Delta G'$ in Figure 3B) is not

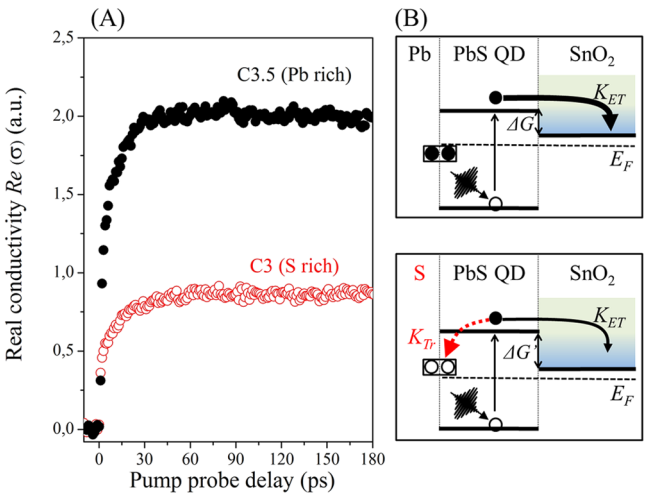

Figure 3. Stoichiometry effect on ET dynamics. (A) Characteristic optical pump−THz probe response for PbS QDs sensitizing SnO_2 by SILAR as a function of surface stoichiometry (comparing samples with C3 and C3.5 SILAR cycles). (B) Sketch illustrating system energetics as a function of PbS QD surface stoichiometry (ΔG represents donor−acceptor ET driving force); S-rich QD surfaces are populated with acceptors (p-type) allowing electron trapping (K_{Tr}) at the nanocrystal surface; Pb-rich surfaces are populated by donors (n-type), making electron trapping at the surface not feasible and hence maximizing the probability of ET to the oxide (K_{ET}).

modulated by QD size or surface doping (ΔG and $\Delta G'$ are equal and independent of nanocrystal dimensions). This is generally different from ex situ QD-sensitized oxide systems, where ET slows down with increasing QD size as a consequence of reduced ΔG (see Figure 3B).[33,34,44] Similarly, as theoretically predicted[45] and experimentally reported,[27,29,46] changes in the SILAR QD S/Pb ratio (QD stoichiometry) will affect the QD Fermi level, yet apparently do not affect ET rates. While the variation in both QD size and stoichiometry will affect QD energy levels, the energy difference between QD LUMO and oxide CB is not modulated by QD size or doping at the QD/air interface.

Back ET (BET) kinetics have been reported[47,48] in dye sensitized systems to be determined by not only the energetics, but also by diffusion/hopping of charges within the oxide films, which can also be rate limiting. Even in the simple case that the overall recombination is determined by the interfacial BET, and assuming Marcus theory applies, BET rates will vary with driving force in a way depending on whether it occurs on the normal or inverted regions (which will depend on the system reorganization energy). Also BET can be a function of oxide/QD coupling strength which in our system is QD size dependent.[20] Although an accurate description of the BET process observed here is out of the scope of the present work, the observed decrease of K_{BET} with SILAR-cycle-number (see inset Figure 2A) is consistent with an upward-shifting HOMO level (the HOMO level is not pinned). The experimentally resolved decrease of K_{BET} with SILAR-cycle-number (see inset Figure 2A) is then a consequence of an increasingly smaller driving force for BET and increasingly smaller donor/acceptor coupling with increasing QD size.

Dependence of ET Efficiency on QD Size and Stoichiometry. Theoretically,[45] nanocrystals with a perfect 1:1 stoichiometry ratio are expected to be intrinsic and therefore defect free. In practice, synthesized nanocrystals are typically nonstoichiometric[28,49−51] and characterized by the presence of surface states acting as donors or acceptors.[45] The passivation of those states for SILAR-based QDs requires a postgrowth passivation treatment, commonly accomplished by introducing an organic or inorganic capping shell onto the QDs.[3,25,52] Alternatively, atomic passivation has been successfully exploited as a pathway for reversibly[31,53] tailoring the optoelectronic properties in colloidal QD solids, through doping[27−30,45,46] and passivation.[31,53−55] The effect of stoichiometry on QD-sensitized oxide systems has not been addressed to date. In Figure 3A, we plot the ET dynamics for PbS QDs nucleated onto SnO_2 nanoparticles by C3 and C3.5 SILAR cycles (probed on the same sample spot for a given oxide substrate), corresponding to S- and Pb-rich QD surfaces, respectively. From the obtained plateau amplitude of the ET traces it is evident that QDs terminated by Pb surfaces allow more efficient ET from the QD to the oxide than those terminated by S (assuming that half cycle treatment by itself is not sufficient for the nucleation of new dots). This finding is consistent with the removal of PbS QD surface acceptors acting as traps by Pb capping and is in perfect agreement with theory and experiments reporting the generation of Pb-related surface donors on QDs with S/Pb < 1 ratios.[29,45,46] As summarized in Figure 3B, the observed enhancement of ET efficiency for lead-rich (or sulfur-deficient) QD surfaces is a manifestation of a favorable kinetic competition between QD-oxide electron transfer (K_{ET}) and undesired trapping at the QD surface (K_{Tr}). Analogously, a sulfur-rich (lead-deficient) QD surface will be prone to trapping of photogenerated electrons in surface acceptor traps, lowering the ET efficiency.

The half cycle-cation passivation effect reported here for the PbS/SnO_2 system is a general phenomenon, as we observed identical qualitative effects on half-cycle terminated samples consisting on PbS/TiO_2, PbS/ZnO, and PbSe/SnO_2 (see Figure S9 in Supporting Information).

In Figure 4A, we present the maximum of the observed pump-induced real photoconductivity (Re(σ) at ~100 ps after the excitation pulse) as a function of the number of SILAR cycles for PbS nanocrystals sensitizing SnO_2. As already discussed for C3 and C3.5 SnO_2/PbS samples (Figure 3A), the passivation effect by an additional half cycle results in an ET efficiency enhancement in all cases (from C1.5/C1 to C6.5/C6). For atomically Pb-passivated samples we resolve a monotonous increase in the monitored photoconductivity as a function of SILAR cycles within the range defined by C1.5 and C4.5. For samples treated beyond C4.5 SILAR cycles (C5.5 and C6.5 SILAR cycles), a decay in the overall measured photoconductivity is observed. The decay is consistent with the formation of QD aggregates beyond C4 cycles as discussed previously (bulky PbS phases acting as strong photon absorbers but poor donors). The observed improvement in the absolute amplitude of the photoconductivity between C1.5 and C4.5 SILAR cycles can be correlated with a QD size-dependent effect but can also result from an increasing population of QDs per unit area. In order to remove the potential effect of an

dx.doi.org/10.1021/nl5026634 | Nano Lett. 2014, 14, 5780−5786

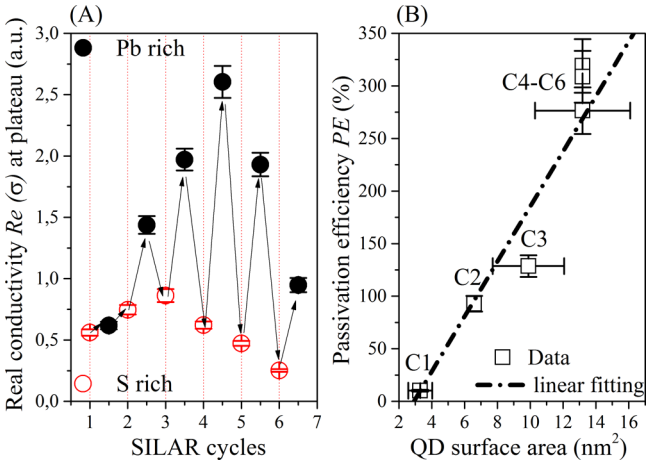

Figure 4. (A) Monitored real conductivity at the plateau (when ET has ended) as a function of SILAR deposition steps. Samples made of complete- and half-cycles are characterized by S- and Pb-rich QD surfaces. (B) Atomic passivation efficiency (PE) versus QD surface area (estimated from TEM statistics and the epitaxial growth model as discussed in the paper). The uncertainty in PE is obtained from 5 to 7 measurements on a given sample (see Figure S6B in Supporting Information). The uncertainty in the QD surface area is inferred from the distribution in QD base diameter (fwhm) as a function of SILAR cycles from TEM analysis.

increasing QD population, we define here a passivation efficiency term defined as PE = $\{\mathrm{Re}(\sigma)_{Cn.5} - \mathrm{Re}(\sigma)_{Cn})/\mathrm{Re}(\sigma)_{Cn}\}$, with $n \geq 1$, where $\mathrm{Re}(\sigma)_{Cn.5}$ and $\mathrm{Re}(\sigma)_{Cn}$ stand for the plateau real conductivity of samples with C*n*.5 and C*n* SILAR cycles, respectively. In this respect, PE simply represents the Pb-passivation effect without considering changes in QD surface densities per unit area of the oxide. As derived in the Supporting Information (section 3.6), the passivation efficiency can be rewritten as PE = $\{K_{Tr}/K_{ET}\}$ in which K_{Tr} represents the rate of electron trapping at QD surfaces and K_{ET} is the rate of ET from donor to acceptor. As a consequence, the defined PE term physically represents the kinetic competition between undesired trapping at the QD surface (K_{Tr}) and QD-oxide electron transfer (K_{ET}), as illustrated in Figure 3B. As discussed above (see Figure 2A), K_{ET} is constant regardless of QD size (or, equivalently, regardless of the number of SILAR cycles, C*n*). On the other hand, trapping rates are linearly dependent on defect density in bulk semiconductors.[S6,S7] In this respect, for our system (where $K_{ET}(Cn)$ = constant) we have that PE $\propto$ $K_{Tr}(Cn) \propto N_{acceptors} \propto QD_{surface\ area}$. In Figure 4B, the dependence of PE versus $QD_{surface\ area}$ is plotted, the latter being estimated from our epitaxial model and TEM characterization, see Figure 1D,E,G. A linear correlation is resolved between C1 and C4 SILAR cycles, which is in agreement with the notion that the QD trapping rate is linearly correlated with QD area. Note that the saturation of PE at 300% versus QD surface area observed for samples beyond C4 is a manifestation of the saturation in the QD size as a function of deposition steps (in perfect agreement with TEM characterization).

Implications of Our Results for QDSSC Design. The maximum theoretical efficiency in excitonic solar cells is given by the Shockley–Queisser limit, provided that efficient ET processes from a bandgap optimized sensitizer to the selective contacts are made at no energy cost[19] (i.e., ohmic contacts are established between the sensitizer HOMO–LUMO levels and the electron–hole electrodes, respectively). In this contribution, we show that stoichiometry control on SILAR-based QDs can be employed as a simple and efficient passivation scheme in order to remove recombination pathways in the QD sensitizers (an essential requirement for devices with high photocurrents). Provided that full passivation in the QDs is achieved by half SILAR cycle treatments (e.g., atomic passivation will not be compromised by surface packing as may be the case for molecules), the only electron relaxation pathway in the QDs will be radiative, making the kinetic competition with ET to the oxide favorable for the latter. On the other hand, we have resolved saturation in QD size during growth, followed by the appearance of polycrystalline phases as a function of SILAR cycles and suggested Fermi-level pinning at the QD/oxide interface. All these aspects represent constraints toward high-efficiency devices. Saturation in QD size nucleation for a given system (most likely correlated with strain relaxation on lattice mismatched QD and oxide phases) could prevent achieving optimum bandgaps matching the solar spectrum (~1.4 eV for maximum efficiency[19]). Once QD size saturation is reached after a certain number of cycles, the appearance of bulky polycrystalline phases should be prevented in devices (as these are strong photon absorbers and recombination centers without substantially contributing to the photocurrent in the photovoltaic device). Note that preventing the formation of QD aggregates could dictate a minimum thickness to achieve full sunlight absorption for a given QD/oxide system (e.g., if QD oxide coverage depends on the number of deposited SILAR cycles). Finally, the suggested pinning at QD/oxide surfaces could prevent fine-tuning of donor–acceptor energetics, and then trying to achieve ohmic contacts between QD and oxide will be compromised (potentially reducing solar cell output voltage[19]).

In order to check whether metallic surfaces will constrain the voltage in devices and also whether the monitored passivation efficiency can be exploited in complete devices (e.g., if such an effect is unaltered by the presence of a hole conductor), we characterized three sets of QDSSCs based on 4 and 4.5 PbS QD SILAR cycles onto TiO_2 electrodes (C4 and C4.5 samples, respectively). The ITO/PbS@TiO_2 electrodes where covered with spiro-OMeTAD/Au contacts (further details are given in the Supporting Information) and solar cell current–voltage characteristics were recorded in a homemade solar simulator. As shown in Figure 5A, for all the devices tested we obtained a ~210% improvement in the photocurrent for the samples terminated with half a cycle (Pb-rich QD surfaces), revealing a quantitative correlation between the observed PE improvement by OPTP measurements (see Figure 5B) and the monitored short circuit current (J_{sc}) in complete solar cell devices. Note that the kinetics (including recombination kinetics) may differ substantially under transient (THz) and steady-state (device working) conditions (under illumination). In particular, under steady-state illumination trap filling can alter transfer rates. On the other hand, we observe that the open circuit voltages (V_{oc}) for the two devices containing, respectively, QDs with Pb- or S-rich surfaces are indistinguishable within the range of values observed for the different samples. For our cells, the similar values for V_{oc}'s (within the sample-to-sample variation) indicate in simple terms, that the maximum quasi Fermi level splitting under illumination within the PbS QD absorber (which could be limited by the reported pinning) is preserved for cationic and anionic rich QD surfaces. Overall, the reported results indicate that atomic passivation can potentially be very well-suited for QDSSCs.

dx.doi.org/10.1021/nl5026634 | Nano Lett. 2014, 14, 5780–5786

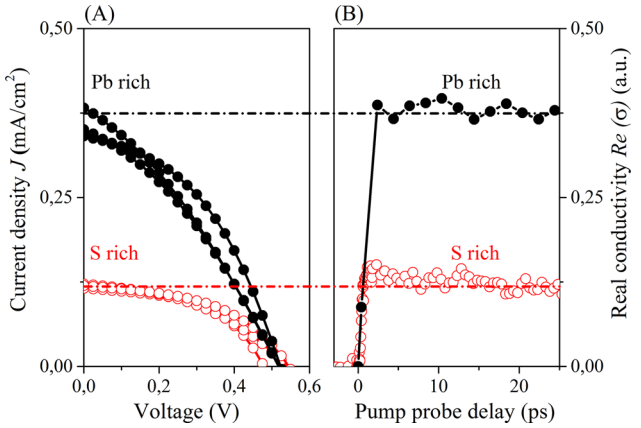

Figure 5. (A) Current−voltage characteristics of QDSSC devices (ITO/PbS@TiO_2/spiro-OMeTAD/Au) with QDs terminated with a lead- or sulfur-rich surface; (B) characteristic optical pump-THz probe response for PbS QDs sensitizing TiO_2 by SILAR as a function of surface stoichiometry (comparing samples with C4 and C4.5 SILAR cycles).

In summary, we have correlated the structure and stoichiometry of QDs grown on SnO_2 films with the electron transfer rates and efficiency. Transmission electron microscopy reveals saturation in the QD base diameter, followed by an increase in nanocrystal height as a function of the number of SILAR cycles. This shape transition, together with the observation of the presence of heteroepitaxial nucleated dots, suggests that Volmer−Weber growth (mediated by lattice mismatch between QD and oxide materials), is the underlying growth mechanism for the analyzed SILAR-based QD sensitized system. While ET rates from the QD to the oxide are found to be insensitive to QD size and stoichiometry (attributed to Fermi level pinning at the QD/oxide interface), the ET efficiency is found to be highly dependent on both aspects. In fact, half-cycle, n-type QD surfaces (cation-rich) exhibit a better passivation of the QD, which in turn favors photoinduced ET processes from the QD to the oxide acceptor. The cationic passivation effect is found to be QD-size dependent, being more prominent as QD area increases and correlating with density of QD surface acceptors. Finally, OPTP measurements are correlated with device photocurrents, showing that exploiting QD stoichiometry for nanocrystal passivation could be an efficient strategy for solar cell design.

■ ASSOCIATED CONTENT

Supporting Information

Sample preparation details: oxide films; sensitization of oxides films with PbS by SILAR; solar cell device fabrication. Sample characterizations: diffuse reflectance; transmission electron microscopy; optical pump-THz probe spectroscopy, sample to sample reproducibility; QD oxidation effects on ET dynamics; ET versus SILAR cycles; lead cation passivation effects on different oxides; definition of passivation efficiency; and estimate of optical pump-THz probe sensitivity. This material is available free of charge via the Internet at http://pubs.acs.org.

■ AUTHOR INFORMATION

Corresponding Author

*E-mail: Canovas@mpip-mainz.mpg.de.

Author Contributions

H.W. and I.B. contributed equally to this work.

Notes

The authors declare no competing financial interest.

■ ACKNOWLEDGMENTS

This work has been financially supported by the Max Planck Society. H.W. is a recipient of a fellowship of the Graduate School Materials Science in Mainz (MAINZ) funded through the German Research Foundation in the Excellence Initiative (GSC 266). The authors acknowledge C. H. Weng and S. Kraus for device preparation and characterization, and C. Almansa for TEM measurements. I.B. is grateful to the Materials Science Doctoral program of the Universitat d'Alacant (UA) for the award of a travel grant. The UA team acknowledges the financial support from the Spanish Ministry of Economy and Competitiveness through project MAT2012-37676 (FONDOS FEDER).

■ REFERENCES

(1) Pan, Z.; Mora-Seró, I.; Shen, Q.; Zhang, H.; Li, Y.; Zhao, K.; Wang, J.; Zhong, X.; Bisquert, J. *J. Am. Chem. Soc.* **2014**, *136*, 9203−9210.
(2) Wang, J.; Mora-Seró, I.; Pan, Z.; Zhao, K.; Zhang, H.; Feng, Y.; Yang, G.; Zhong, X.; Bisquert, J. *J. Am. Chem. Soc.* **2013**, *135*, 15913−15922.
(3) Santra, P. K.; Kamat, P. V. *J. Am. Chem. Soc.* **2012**, *134*, 2508−2511.
(4) Lee, H.; Wang, M.; Chen, P.; Gamelin, D. R.; Zakeeruddin, S. M.; Grätzel, M.; Nazeeruddin, M. K. *Nano Lett.* **2009**, *9*, 4221−4227.
(5) Rühle, S.; Shalom, M.; Zaban, A. *ChemPhysChem* **2010**, *11*, 2290−2304.
(6) Lee, J.-W.; Son, D.-Y.; Ahn, T. K.; Shin, H.-W.; Kim, I. Y.; Hwang, S.-J.; Ko, M. J.; Sul, S.; Han, H.; Park, N.-G. *Sci. Rep.* **2013**, *3*, 1050.
(7) Ahn, H.-J.; Kim, M.-J.; Kim, K.; Kwak, M.-J.; Jang, J.-H. *Small* **2014**, *10*, 2325−2330.
(8) Kim, K.; Kim, M.-J.; Kim, S.-I.; Jang, J.-H. *Sci. Rep.* **2013**, 3.
(9) Su, F.; Lu, J.; Tian, Y.; Ma, X.; Gong, J. *Phys. Chem. Chem. Phys.* **2013**, *15*, 12026−12032.
(10) Salant, A.; Shalom, M.; Hod, I.; Faust, A.; Zaban, A.; Banin, U. *ACS Nano* **2010**, *4*, 5962−5968.
(11) Blackburn, J. L.; Selmarten, D. C.; Nozik, A. J. *J. Phys. Chem. B* **2003**, *107*, 14154−14157.
(12) Piris, J.; Ferguson, A. J.; Blackburn, J. L.; Norman, A. G.; Rumbles, G.; Selmarten, D. C.; Kopidakis, N. *J. Phys. Chem. C* **2008**, *112*, 7742−7749.
(13) Guijarro, N.; Lana-Villarreal, T.; Shen, Q.; Toyoda, T.; Gomez, R. *J. Phys. Chem. C* **2010**, *114*, 21928−21937.
(14) Wang, H.; McNellis, E. R.; Kinge, S.; Bonn, M.; Cánovas, E. *Nano Lett.* **2013**, *13*, 5311−5315.
(15) Selinsky, R. S.; Shin, S.; Lukowski, M. A.; Jin, S. *J. Phys. Chem. Lett.* **2012**, *3*, 1649−1656.
(16) Acharya, K. P.; Khon, E.; O'Conner, T.; Nemitz, I.; Klinkova, A.; Khnayzer, R. S.; Anzenbacher, P.; Zamkov, M. *ACS Nano* **2011**, *5*, 4953−4964.
(17) Selinsky, R. S.; Ding, Q.; Faber, M. S.; Wright, J. C.; Jin, S. *Chem. Soc. Rev.* **2013**, *42*, 2963−2985.
(18) Acharya, K. P.; Hewa-Kasakarage, N. N.; Alabi, T. R.; Nemitz, I.; Khon, E.; Ullrich, B.; Anzenbacher, P.; Zamkov, M. *J. Phys. Chem. C* **2010**, *114*, 12496−12504.
(19) Giebink, N. C.; Wiederrecht, G. P.; Wasielewski, M. R.; Forrest, S. R. *Phys. Rev. B* **2011**, *83*, 195326.
(20) Tisdale, W. A.; Zhu, X.-Y. *Proc. Nat. Acad. Sci. U.S.A.* **2011**, *108*, 965−970.
(21) Yang, Y.; Rodríguez-Córdoba, W.; Xiang, X.; Lian, T. *Nano Lett.* **2011**, *12*, 303−309.

(22) Nicolau, Y. F. *Appl. Surf. Sci.* **1985**, *22*−*23*, 1061−1074.
(23) Park, S.; Clark, B. L.; Keszler, D. A.; Bender, J. P.; Wager, J. F.; Reynolds, T. A.; Herman, G. S. *Science* **2002**, *297*, 65.
(24) Barcelo, I.; Campina, J. M.; Lana-Villarreal, T.; Gomez, R. *Phys. Chem. Chem. Phys.* **2012**, *14*, 5801−5807.
(25) Lee, H.; Leventis, H. C.; Moon, S.-J.; Chen, P.; Ito, S.; Haque, S. A.; Torres, T.; Nüesch, F.; Geiger, T.; Zakeeruddin, S. M.; Grätzel, M.; Nazeeruddin, M. K. *Adv. Funct. Mater.* **2009**, *19*, 2735−2742.
(26) Lee, H. J.; Chen, P.; Moon, S.-J.; Sauvage, F.; Sivula, K.; Bessho, T.; Gamelin, D. R.; Comte, P.; Zakeeruddin, S. M.; Seok, S. I.; Grätzel, M.; Nazeeruddin, M. K. *Langmuir* **2009**, *25*, 7602−7608.
(27) Kim, D. K.; Fafarman, A. T.; Diroll, B. T.; Chan, S. H.; Gordon, T. R.; Murray, C. B.; Kagan, C. R. *ACS Nano* **2013**, *7*, 8760−8770.
(28) Luther, J. M.; Pietryga, J. M. *ACS Nano* **2013**, *7*, 1845−1849.
(29) Oh, S. J.; Berry, N. E.; Choi, J.-H.; Gaulding, E. A.; Lin, H.; Paik, T.; Diroll, B. T.; Muramoto, S.; Murray, C. B.; Kagan, C. R. *Nano Lett.* **2014**, *14*, 1559−1566.
(30) Engel, J. H.; Alivisatos, A. P. *Chem. Mater.* **2013**, *26*, 153−162.
(31) Thon, S. M.; Ip, A. H.; Voznyy, O.; Levina, L.; Kemp, K. W.; Carey, G. H.; Masala, S.; Sargent, E. H. *ACS Nano* **2013**, *7*, 7680−7688.
(32) Li, J. J.; Wang, Y. A.; Guo, W.; Keay, J. C.; Mishima, T. D.; Johnson, M. B.; Peng, X. *J. Am. Chem. Soc.* **2003**, *125*, 12567−12575.
(33) Cánovas, E.; Moll, P.; Jensen, S. A.; Gao, Y.; Houtepen, A. J.; Siebbeles, L. D. A.; Kinge, S.; Bonn, M. *Nano Lett.* **2011**, *11*, 5234−5239.
(34) Canovas, E.; Pijpers, J.; Ulbricht, R.; Bonn, M. Carrier Dynamics in Photovoltaic Structures and Materials Studied by Time-Resolved Terahertz Spectroscopy. In *Solar Energy Conversion: Dynamics of Interfacial Electron and Excitation Transfer*; The Royal Society of Chemistry: London, 2013; Chapter 11, pp 301−336.
(35) Pijpers, J. J. H.; Koole, R.; Evers, W. H.; Houtepen, A. J.; Boehme, S.; de Mello Donegá, C.; Vanmaekelbergh, D.; Bonn, M. *J. Phys. Chem. C* **2010**, *114*, 18866−18873.
(36) Pijpers, J. J. H.; Ulbricht, R.; Derossi, S.; Reek, J. N. H.; Bonn, M. *J. Phys. Chem. C* **2011**, *115*, 2578−2584.
(37) Ulbricht, R.; Hendry, E.; Shan, J.; Heinz, T. F.; Bonn, M. *Rev. Mod. Phys.* **2011**, *83*, 543−586.
(38) Barceló, I.; Lana-Villarreal, T.; Gómez, R. *J. Photochem. Photobiol., A* **2011**, *220*, 47−53.
(39) Müller, P.; Kern, R. *J. Cryst. Growth* **1998**, *193*, 257−270.
(40) Ferreira, S. O.; Neves, B. R. A.; Magalhães-Paniago, R.; Malachias, A.; Rappl, P. H. O.; Ueta, A. Y.; Abramof, E.; Andrade, M. S. *J. Cryst. Growth* **2001**, *231*, 121−128.
(41) Wang, F.; Shan, J.; Islam, M. A.; Herman, I. P.; Bonn, M.; Heinz, T. F. *Nat. Mater.* **2006**, *5*, 861−864.
(42) Markus, T. Z.; Itzhakov, S.; Alkotzer, Y. I.; Cahen, D.; Hodes, G.; Oron, D.; Naaman, R. *J. Phys. Chem. C* **2011**, *115*, 13236−13241.
(43) Walther, C.; Blum, R. P.; Niehus, H.; Masselink, W. T.; Thamm, A. *Phys. Rev. B* **1999**, *60*, R13962−R13965.
(44) Kongkanand, A.; Tvrdy, K.; Takechi, K.; Kuno, M.; Kamat, P. V. *J. Am. Chem. Soc.* **2008**, *130*, 4007−4015.
(45) Kim, D.; Kim, D.-H.; Lee, J.-H.; Grossman, J. C. *Phys. Rev. Lett.* **2013**, *110*, 196802.
(46) Oh, S. J.; Berry, N. E.; Choi, J.-H.; Gaulding, E. A.; Paik, T.; Hong, S.-H.; Murray, C. B.; Kagan, C. R. *ACS Nano* **2013**, *7*, 2413−2421.
(47) Weng, Y.-S.; Wang, Y.-Q.; Asbury, J. B.; Ghosh, H. N.; Lian, T. *J. Phys. Chem. B* **2000**, *104*, 93−104.
(48) Green, A. N. M.; Palomares, E.; Haque, S. A.; Kroon, J. M.; Durrant, J. R. *J. Phys. Chem. B* **2005**, *109*, 12525−12533.
(49) Anderson, N. C.; Hendricks, M. P.; Choi, J. J.; Owen, J. S. *J. Am. Chem. Soc.* **2013**, *135*, 18536−18548.
(50) Petkov, V.; Moreels, I.; Hens, Z.; Ren, Y. *Phys. Rev. B* **2010**, *81*, 241304.
(51) Moreels, I.; Lambert, K.; De Muynck, D.; Vanhaecke, F.; Poelman, D.; Martins, J. C.; Allan, G.; Hens, Z. *Chem. Mater.* **2007**, *19*, 6101−6106.
(52) de la Fuente, M. S.; Sánchez, R. S.; González-Pedro, V.; Boix, P. P.; Mhaisalkar, S. G.; Rincón, M. E.; Bisquert, J.; Mora-Seró, I. *J. Phys. Chem. Lett.* **2013**, *4*, 1519−1525.
(53) Voznyy, O.; Zhitomirsky, D.; Stadler, P.; Ning, Z.; Hoogland, S.; Sargent, E. H. *ACS Nano* **2012**, *6*, 8448−8455.
(54) Wei, H. H. Y.; Evans, C. M.; Swartz, B. D.; Neukirch, A. J.; Young, J.; Prezhdo, O. V.; Krauss, T. D. *Nano Lett.* **2012**, *12*, 4465−4471.
(55) Jasieniak, J.; Mulvaney, P. *J. Am. Chem. Soc.* **2007**, *129*, 2841−2848.
(56) Lambsdorff, M.; Kuhl, J.; Rosenzweig, J.; Axmann, A.; Schneider, J. *Appl. Phys. Lett.* **1991**, *58*, 1881−1883.
(57) Doany, F. E.; Grischkowsky, D.; Chi, C. C. *Appl. Phys. Lett.* **1987**, *50*, 460−462.